Review

A Review of Wireless Power Transfer Systems for Electric Vehicle Battery Charging with a Focus on Inductive Coupling

Iman Okasili, Ahmad Elkhateb * and Timothy Littler

School of Electronics, Electrical Engineering and Computer Science (EEECS), Queen's University, Belfast BT9 5AH, UK; iokasili01@qub.ac.uk (I.O.); t.littler@qub.ac.uk (T.L.)
* Correspondence: a.elkhateb@qub.ac.uk

Abstract: This article classifies, describes, and critically compares different compensation schemes, converter topologies, control methods, and coil structures of wireless power transfer systems for electric vehicle battery charging, focusing on inductive power transfer. It outlines a path from the conception of the technology to the modern and cutting edge of the technology. First, the base principles of inductive coupling power transfer are supplied to give an appreciation for the operation and design of the systems. Then, compensation topologies and soft-switching techniques are introduced. Reimagined converter layouts that deviate from the typical power electronics topologies are introduced. Control methods are detailed alongside topologies, and the generalities of control are also included. The paper then addresses other essential aspects of wireless power transfer systems such as coil design, infrastructure, cost, and safety standards to give a broader context for the technology. Discussions and recommendations are also provided. This paper aims to explain the technology, its modern advancements, and its importance. With the need for electrification mounting and the automotive industry being at the forefront of concern, recent advances in wireless power transfer will inevitably play an essential role in the coming years to propel electric vehicles into the common mode of choice.

Keywords: electric vehicles; inductive power transfer; battery chargers; wireless power transfer; compensation; converters; static systems; dynamic systems

1. Introduction

As sustainability becomes a greater focus in the global community, the electrification of industries is on the rise. Electrification offers sectors that traditionally are heavy polluters the opportunity to source their energy from more sustainable means. The automotive industry is at the forefront of this new wave of electrification but faces significant challenges in adopting electric vehicles (EV). Wireless power transfer (WPT) offers a means of mitigating the issues of range-per-charge and time-to-charge for EVs. Since expectations grow for the electrification of the automotive industry, pressure is mounting on manufacturers to enhance and improve EV technology. Two of the most significant challenges in adopting EVs are the issues of range and charging times. Compared to internal combustion engine (ICE) vehicles, EVs have traditionally had a smaller range in the distance travelled per charge/refuel. This is due to the energy density difference of modern batteries against that of petroleum and other fossil fuel sources. The energy density of standard gasoline is around 8200 Wh/kg, over 10 times greater than that of mature EV battery technology [1] and still over double that of emerging technologies [2]. The glaring issues of EV use are exacerbated in long journeys because of the need to stop more often for recharging. The problem has historically been compounded by the fact that ICE vehicles only take a few minutes to refuel which in many cases was and is still far faster than the time needed to significantly charge an EV. In [3] a comparison of state-of-the-art extreme fast DC chargers is given. It is reported that at the peak end, systems can supply enough charge to power the

vehicle for around 200 miles in as little 10 min. However, this still remains the extreme case and the same report details current high-end charging at around 25 min and over. Whilst researchers are improving EVs by increasing efficiency and developing better batteries, there has long been speculation on how to improve infrastructure to mitigate some of the technology's inherent limitations. WPT has been theorized for EVs for over 100 years [4] to increase range. In the past 20–30 years, WPT for EVs has taken significant leaps in modernizing the technology. There are two main categories to the technology, which are static and dynamic charging. As the names imply, static charging is available when the vehicle is stationary and dynamic charging is the process of supplying power to an EV while it is moving. Early systems for WPT for EVs focused more on dynamic charging. The work in [5] is one of the earliest proposals of roadway powered EVs (RPEVs). RPEVs are EVs that derive all their energy from a primary side inductor implanted into the driving surface received by a secondary inductor in the vehicle, thus limiting the journey range to the length of the powered driving surface. This concept heavily inspired researchers, and so, research began on the modern concept in 1990 [6]. One of the most significant contributors to the field of dynamic WPT are researchers at the University of Auckland; their work in the early 2000's pioneered many important concepts [7–10]. The Korean Advanced Institute of Science and Technology is also notable in this department with its work on online electric vehicles (OLEVs). OLEVs are a hybrid of traditional battery dependent EVs and RPEVs. The concept of an OLEV is to reduce battery size whilst still maintaining a suitable range for standard driving. This technology has been shown to need around 20% of the battery capacity of their plug-in charger counterparts [11]. With WPT systems having already achieved power transfer over air gaps of up to 200 mm, and efficiencies of approximately 96% [12], the feasibility of the technology is being certified. This paper presents an overview of WPT systems advancements whilst highlighting important milestones and challenges faced by researchers. The paper will begin with a recap of the fundamentals of WPT systems to propagate a better understanding of past advancements in the field and contemporary work. The paper will then address research in crucial areas, referring to compensation schemes, control methods, converter topologies and coil design. This paper will also detail broader topics such as safety standards and costs before finally reflecting on the current technology with speculation on future systems.

2. Fundamentals of WPT Systems

This section will detail the base principles on which modern WPT transfer systems are built, including a derivation of mutual inductance and coupling factor. A detailed explanation of reflection is included to support the basic power transfer and efficiency equations presented. This section illustrates key principles so as to supply a better context for the challenges faced and the breakthroughs achieved in WPT.

2.1. Overall Systems Configuration

This paper focuses on WPT systems that make use of the inductive coupling method. Inductively coupled power transfer (ICPT) systems use the generated magnetic field from an inductor subject to a change in current as a means for transferring power wirelessly. A typical WPT system consists of a primary and secondary side coupled by inductors. A precursor to the system involves rectifying the domestic supply, and DC-DC conversion takes place with power factor correction so that the system is supplied with a suitable voltage. On the primary side of the system, there is an inverter for creating an AC waveform to drive the coupled inductor network. Compensation schemes are employed on either side of the inductors. The high-frequency output of the inverter is used to generate a magnetic field from the primary winding, which in turn induces an AC current in the secondary. The frequency used can be selected to resonate with the secondary compensations scheme to significantly improve power transfer and efficiency. The waveform is then rectified to charge the battery.

2.2. Mutual Inductance and Coupling Factor

The operating principle of ICPT is like that of a transformer in several aspects. The significant divergence is the lack of a fully formed ferrite core. In the case of ICPT, there is a significant air gap present between the primary and secondary windings. Thus, the principles of operation differ as the coupling factor is far below 1. The operation of a WPT system is heavily dependent on the mutual inductance M; mutual inductance is linked to how well the system is coupled which is commonly referred to as the coupling factor k. From [13], we can derive expressions for M and k. When initially subjected to a DC current, an inductor stores energy in its winding; 0 current is passing through the coils at time $t = 0$, and a growing/changing current i_1 is first seen in the primary coil until it reaches its peak at time $t = t_2$. Due to this growing/changing current in the primary, the secondary has an induced current i_2 that follows the same trend over time as i_1. For the case of energizing a pair of mutually coupled inductors with a DC current, the energy stored, W, during the charge time, can be calculated using (1):

$$W|_{t_0}^{t_2} = \frac{1}{2}L_1 i_1{}^2 \pm M i_1 i_2 + \frac{1}{2}L_2 i_2{}^2 \tag{1}$$

As seen in Figure 1, L_1, L_2 and i_1, i_2 are the self-inductances and currents of the primary and secondary, respectively.
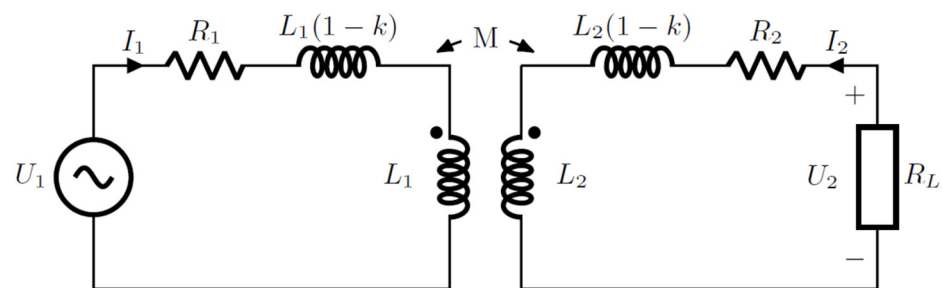

Figure 1. Basic Inductive Power Transfer System with leakage inductance.

The energy in the system cannot be negative, so to gain a definition for M, we can exploit this by assuming that the M term is negative:

$$W|_{t_0}^{t_2} = \frac{1}{2}L_1 i_1{}^2 + \frac{1}{2}L_2 i_2{}^2 - M i_1 i_2 \tag{2}$$

Adding and subtracting the term $\sqrt{L_1 L_2} i_1 i_2$ to Equation (2) will allow for completing the square to give (3):

$$W|_{t_0}^{t_2} = \frac{1}{2}\left(\sqrt{L_1} i_1 - \sqrt{L_2} i_2\right)^2 + \sqrt{L_1 L_2} i_1 i_2 - M i_1 i_2 \tag{3}$$

The first term on the right-hand side can approach 0 but cannot be negative, so for the energy transfer to be positive, the definition of M must be:

$$\sqrt{L_1 L_2} \geq M \tag{4}$$

The ratio of $M/\sqrt{L_1 L_2}$ is known as the coefficient of coupling or coupling factor k:

$$k = \frac{M}{\sqrt{L_1 L_2}} \tag{5}$$

and k can be any value between 0 and 1, $0 \leq k \leq 1$. The coupling factor is the ratio of flux linkage between the primary and secondary coils. Figure 1 depicts how the coupling factor is modelled as a circuit to represent the non-linked flux or flux leakage.

2.3. Reflection

The nature of the system is such that as the primary causes an induced current in the secondary, the secondary also has an opposing effect on the primary. The voltage induced in the secondary by the primary current i_1 is stated as $j\omega M i_1$ and the reflected voltage from the secondary current i_2 onto the primary can be stated as $-j\omega M i_2$ [14], where ω is the angular frequency expressed as $\omega = 2\pi f$.

Impedance is reflected from the secondary to the primary, and from Kirchhoff's Voltage Law (KVL), we get:

$$Z_{in} = \frac{V_s}{I_1} = j\omega L_1 + \frac{\omega^2 M^2}{j\omega L_2 + Z_{LD}} \tag{6}$$

where Z_{in} and Z_{LD} are the input and load impedance, respectively. The second term of the right-hand side is the result of the mutual coupling and is the reflected impedance Z_r:

$$Z_r = \frac{\omega^2 M^2}{j\omega L_2 + Z_{LD}} \tag{7}$$

The impedance of the secondary $Z_s = j\omega L_2 + Z_{LD}$ so:

$$Z_r = \frac{\omega^2 M^2}{Z_s} \tag{8}$$

We can also express the load impedance as $Z_{LD} = R_{LD} + jX_{LD}$, therefore:

$$Z_r = \frac{\omega^2 M^2}{R_{LD} + j(X_{LD} + \omega L_2)} \tag{9}$$

By rationalizing the denominator, the reflected impedance is expressed in terms of real (Re) and imaginary (Im) parts:

$$Z_r = \frac{\omega^2 M^2 R_{LD}}{R_{LD}^2 + (X_{LD} + \omega L_2)^2} - j\frac{\omega^2 M^2 (X_{LD} + \omega L_2)}{R_{LD}^2 + (X_{LD} + \omega L_2)^2} \tag{10}$$

where:

$$Re\{Z_r\} = \frac{\omega^2 M^2 R_{LD}}{R_{LD}^2 + (X_{LD} + \omega L_2)^2} \tag{11}$$

and:

$$Im\{Z_r\} = -\frac{\omega^2 M^2 (X_{LD} + \omega L_2)}{R_{LD}^2 + (X_{LD} + \omega L_2)^2} \tag{12}$$

The reflected reactance corresponds to the negative of the net reactance of $X_{LD} + \omega L_2$ and, depending on this, it is either capacitive or inductive. Where X_{LD} is capacitive and equal to ωL_2 then the reactance is 0, and the reflected impedance is purely resistive.

2.4. Power Transfer and Efficiency

The power transfer from the primary to the secondary is then stated as the real part of the reflected resistance multiplied by the square of the primary current [14]:

$$P = (ReZ_r)I_1^2 \tag{13}$$

The efficiency of the system is expressed in an equivalent manner as a voltage divider over both the primary and secondary. (14) shows the ratio between the reflect resistance and the resistance of the primary. As power transferred is measured across the reflected resistance, the larger the ratio of reflected resistance in relation to the resistance of the primary the higher the efficiency of the system will be. (15) shows the ratio of load resistance against total secondary side resistance. The greater the ratio of load resistance,

the more power is dissipated across the load in relation to the rest of the circuit during operation:

$$\eta_p = \frac{ReZ_r}{R_p + ReZ_r} \tag{14}$$

$$\eta_s = \frac{R_L}{R_L + R_s} \tag{15}$$

where total efficiency is:

$$\eta_T = \eta_p * \eta_s \tag{16}$$

3. Compensation Schemes

WPT is reliant on coupled inductors as a means of transferring power. Due to the air-core, there can be leakage flux shown in Figures 1 and 2 as $L_x(1 - k)$, which causes the system to be inefficient. Compensation is used to eliminate the presence of leakage flux and improve system performance. In systems where the coupling factor $k > 0.5$, such as a traditional transformer with a ferrite core, the compensation capacitance should resonate with the leakage inductance. Whereas in an air-core system with $k < 0.5$, the compensation capacitance should be resonant with the self-inductance to achieve a zero-phase angle (ZPA) and minimize the reactive part of the reflected impedance. Researchers realized that the adoption of compensation also allowed for control of other parameters. On the primary side, compensation may be used to minimize the VA rating [15] and achieve ZPA so that the real power matches the apparent power. On the secondary side, compensation is constructed for resonance to maximize power transfer. Compensation is also used to employ soft switching via zero voltage switching (ZVS) or zero current switching (ZCS) to minimize power loss in the inverter. Constant current (CC) and constant voltage (CV) can also be realized by compensation [16–18]. This can be used to significantly improve charging, and as such load-independent operation is a highly desirable trait in EV battery charging.
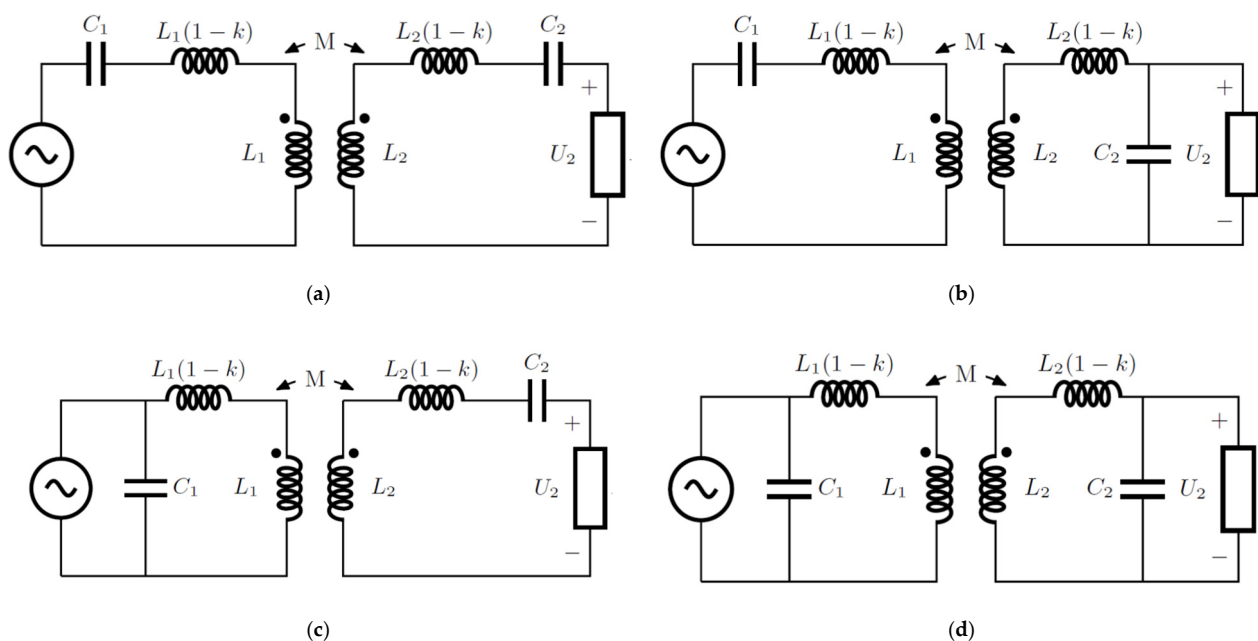

(a)

(b)

(c)

(d)

Figure 2. Four basic compensation topologies: (**a**) SS, (**b**) SP, (**c**) PS and (**d**) PP.

There are four basic topologies of compensation which can be seen in Figure 2, and these are SS, SP, PS and PP, where "S" and "P" stand for series and parallel, respectively. The order in which the "S" or "P" appears denotes their presence on either side of the system. These compensation topologies have been extensively researched [14,16,19,20], and it has been found that SS and SP are the more favorable of the basic topologies, with

some caveats. SS and SP are adequate for reducing the needed rating of the power supply. SP compensation for EV charging is advantageous, as a voltage supplied SP topology was found to have a load-independent output voltage characteristic. However, when SS and SP operate with a voltage source and a no coupling factor situation ($k = 0$) caused by misaligned or large air gaps, it can be unsafe for the power supply [21]. The focus of the basic topologies is to choose a compensation capacitance to eliminate leakage inductance for maximum power transfer. Since a constant voltage is wanted across the load, it can be modelled as constant resistance. The reflected reactance is typically inductive, so any employed compensation should take this into account. Using the reflected impedance theory explained in Section 2 Fundamentals of WPT Systems, it is possible to calculate the compensation capacitances of various topologies [14] to achieve ZPA, which is seen in Table 1. In recent years, researchers have been creating novel forms of compensation to maximize desirable traits. A circuit switching model proposed in [18] used the four basic topologies in a single system. By employing switching techniques to change the compensation topology from one to another, the system could take advantage of of SS and PS simultaneously. [18] also details another system that was able to switch between SP and PP compensation. Practical implementation of this has proved difficult as the CV or CC operation heavily relies on a coupling factor. Higher-order compensation has seen an increase in attention in recent years as topologies have been found to produce desirable characteristics with manageable design constraints. One such example is the double LCL (where 'L' is the presence of an inductor and 'C' is the presence of a capacitor, their respective order is the order in which they appear in the topology) network analyzed in [22–24]. LCL compensation offers protection to the compensating capacitor from the square wave output of the inverter, which subjects the capacitor to large instantaneous changes in voltage, thus impairing its lifespan. It achieves this by placing an inductor after the inverter to curb the fast voltage change. LCL is usually employed on the primary as it not only increases capacitor lifespan but also operates with a constant current that is load-independent with no change concerning varying coupling factors. It can also operate with ZVS and presents some higher-order harmonic filtering. LCC is another topology explored in [25–30] that can realize many of the same benefits as LCL. The proposed tuning method that can operate at a resonant frequency independent of the coupling factor. Both LCL and LCC can achieve DC to DC efficiencies of around 96% at power outputs from 7.36–7.7 kW. Research into hybrid higher-order compensation schemes has proposed an interesting system that uses the first and third harmonic waveforms [31]. The design of the system uses an SS topology for the fundamental waveform and an LCL-S topology for the third harmonic waveform. As described, the output power for both waveforms have an opposing relationship with the system's mutual inductance. A change in mutual inductance causes the output power for one topology to rise and the other to fall. The use of compensation networks in tandem allows for steadier output power and load voltage when faced with a varying coupling factor. A study on divining topologies that exhibit CC and CV operation for higher-order compensation with load-independent output characteristics is in [17].

Table 1. Compensation Topology Characteristics.

Topology	Quality Factor Q	Reflected Resistance	Primary Capacitance	Primary Current at Resonance	Operation Capabilities
SS	$\frac{\omega_0 L_s}{R}$	$\frac{\omega_0 M^2}{R}$	$\frac{C_s L_s}{L_p}$	$\frac{U_i R}{\omega_0 M^2}$	Voltage source at secondary.
SP	$\frac{R}{\omega_0 L_s}$	$\frac{M^2 R}{L_s^2}$	$\frac{C_s L_s^2}{L_p L_s - M^2}$	$\frac{U_i L_s^2}{M^2 R}$	Current source at secondary.
PS	$\frac{\omega_0 L_s}{R}$	$\frac{\omega_0 M^2}{R}$	$\frac{C_s L_s}{\frac{M^4}{L_p C_s L_s R} - L_p}$	$\frac{U_i R}{\omega_0 M^2}$	Voltage source at secondary.
PP	$\frac{R}{\omega_0 L_s}$	$\frac{M^2 R}{L_s^2}$	$\frac{(L_p L_s - M^2) C_s L_s^2}{\frac{M^4 C_s R}{L_s} + (L_p L_s - M^2)^2}$	$\frac{U_i L_s^2}{M^2 R}$	Current source at secondary.
Double LCL	$\frac{R L_s}{\omega_0 L_2{}^2}$	$\frac{M^2 R}{L_2^2}$	$C_1 = \dfrac{1}{\frac{1}{\omega_0^2 L_1} + \frac{1}{\omega_0^2\left[(1-K)L_p\right]}}$	$\frac{U_i}{\omega_0 L_p}\cdot\left[\frac{1}{Q_1} + \left(\frac{L_p}{L_{f1}} - 1\right)\right]$ [23]	CC operation at primary with unity-power-factor at secondary. Can be tuned to achieve ZVS.
Double LCC	$\frac{R L_s}{\omega_0 L_2{}^2}$	$\frac{M^2 R}{L_2^2}$	$C_{f1} = \frac{1}{\omega_0^2 L_{f1}}$ & $C_1 = \frac{1}{\omega_0^2\left(L_p - L_{f1}\right)}$	$\frac{\sqrt{L_1 L_2}}{\omega_0 L_{f1} L_{f2}}\cdot k U_i$ [25]	Can maintain resonance with changing load and/or changing coupling factor. Can be tuned to achieve ZVS.

Where: L_p, L_s, C_p and C_s, are the primary and secondary coils and compensation capacitors, respectively. L_{f1}, C_{f1}, L_{f2} and C_{f2} denote the additional inductors and capacitors on the primary and secondary, respectively. ω_0 is the resonant frequency, $Q_1 = \frac{\omega_0 L_p}{R}$ and U_i is the voltage output from the inverter on the primary.

4. Power Electronics and Control

This section focuses on the control and implementation of the driving hardware present in WPT systems for EV battery charging.

4.1. Converters

There are several types of converters used in WPT systems. Figure 3 depicts the typical arrangement of converters used in systems. On the primary side, converters are used to control the power supply to the system. This is typically accomplished via a rectifier and an inverter working in tandem to output the desired frequencies from a standard mains supply. On the primary side, research on converters is mainly focused on the inverter as it is the driver for the circuit's operation. When designing inverters for WPT systems, the focus is heavily centered on achieving resonance [32–36]. Resonance allows for zero phase angle (ZPA) operation, which drastically increases power transfer efficiency as the reflected reactance of the secondary on the primary is purely resistive, so real power matches apparent power transferred. The switches in the inverter must be rated for the power supply and able to operate at high frequencies. High frequency is needed to transfer high power levels across an air gap. When operating at resonance, the compensation of the system may also function as a filter to higher-order harmonics. In most cases, the waveform supplied to the transmitting coil can be considered a sine wave and circuit parameters are found by first harmonic analysis (FHA). In the case of WPT for EVs, the Society of Automotive Engineers (SAE) have outlined that a bandwidth of 79 kHz − 90 kHz is applicable [37]. On the secondary side of the circuit, the power electronics focus on controlling the load parameters. CV operation is desirable for EV battery charging. Where compensation has allowed for load-independent operation, only a rectifier is needed on the secondary to supply a DC current to the load. In the instances where CV is not an inherent part of the system, a DC-DC converter can be employed on the secondary side to control the voltage across the load [38–40] and can also be used for impedance matching purposes [41]. In many cases, systems can typically operate with four converters. This poses a problem as each converter used has its associated losses and increases the needed space. To combat this, there has been some research conducted into simplifying systems and reducing the number of converters. One such example would be the work in [42], where a direct AC-AC

converter is employed, thus eliminating the need for a primary side rectifier. The proposed system showed the capability to produce a 30 kHz waveform from a 50 Hz source. A promising technology is the class E^2 DC-DC converter which has been proposed for WPT systems in [43–45]. A class E^2 converter offers ZVS and zero derivative switching (ZDS) for the inverter at an optimum load condition $R = R_{opt} = 8/(\pi^2 + 4) * V_I^2/P_o$ where V_I is the input voltage and P_o is the output power. For a range of $0 < R < R_{opt}$, only ZVS is achieved, and for $R_{opt} < R$, neither ZVS nor ZDS are present in operation. It has been shown in [46] that ZVS/ZDS shares a similar condition between coupling factors as with load, where ZVS and ZDS is achieved at an optimum coupling factor K_{opt} and ZVS is apparent in the range of $0 < K < K_{opt}$. Isolated converter topologies have been widely studied and implemented in recent years as a means of ensuring good power quality and safety for devices [47]. As the study of isolated converter topologies has broadened, the technology is speculated for use in WPT. The literature shows that there may be an interesting development in isolated Buck-Boost converter topologies which could make them applicable to a WPT setting. Buck-boost converters allow for the voltage output of the DC-DC converter to be greater or lower than that of the supply. This characteristic is dependent on the duty cycle. There are several Buck-Boost configurations such as Ćuk, Zeta, SEPIC and P5. Several configurations are speculated upon in [48–51], where the consensus is that topologies with split capacitor configurations are better for isolated systems. This is due to their ability to operate with transformer action. In other topologies, energy is transferred via intermediate inductance and exhibits a DC flux bias. Energy transfer is restricted by the core volume, where magnetic energy is temporarily stored in the coupled inductors. The limits of energy storage are related to the hysteresis (BH) curve of the core, where saturation limits dictate the energy storage cap. When a DC flux bias is present, the transformer is only operating in a small portion of the hysteresis curve. In contrast, transformer action makes use of the negative and positive quadrants meaning more energy storage. Thus, this method of intermediate inductance seen in topologies with no split capacitor does not utilize the core as well as immediate transformer action. Topologies with a split capacitor transformer configuration are shown in Figure 4 and can operate without a DC flux bias.
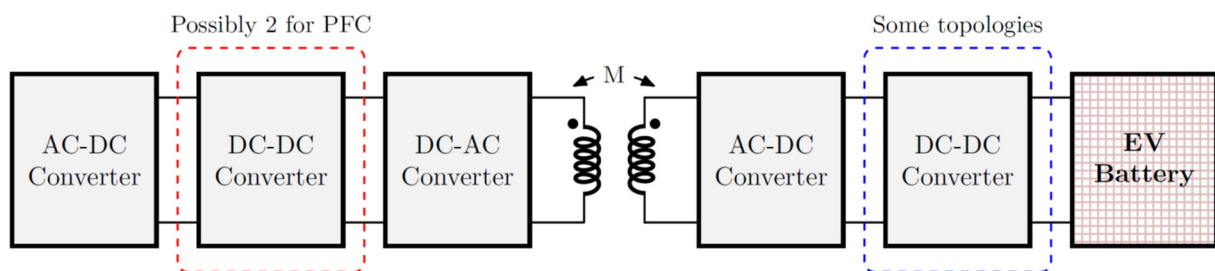

Figure 3. WPT converter topologies. (Where PFC is power factor correction).

The research into these topologies as WPT systems for EV charging is only beginning to gain traction. The work in [51] is the first to consider these converters in a WPT for EV charging setting. The possible benefits of these buck-boost inspired WPT systems are a reduction in total system size and components used. Thus, creating cheaper systems which can be manufactured at greater ease. In recent years it has been speculated that EVs can play an essential role in the decentralization of the grid infrastructure. With renewable energy sources and embedded generation becoming more prevalent, many studies have pointed to EVs as means of mass-energy storage [52,53]. This has prompted the need for bi-directional topologies to facilitate the expedition of electrical energy from the vehicle into the grid [54,55]. This is principally achieved by replacing the secondary side rectifier with a full-bridge inverter, as seen in Figure 5.
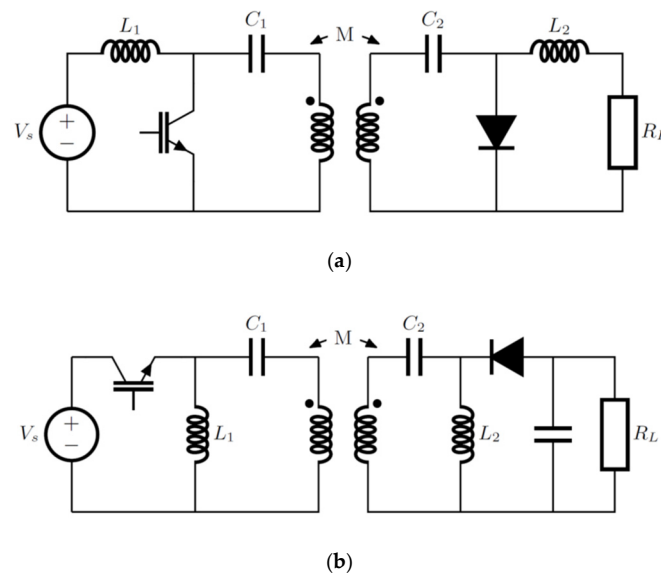
(a)

(b)

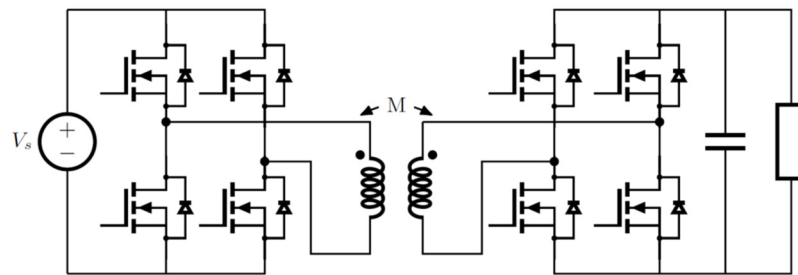**Figure 4.** (**a**) Ćuk converter (**b**) P5 Converter.

Figure 5. Bi-Directional Converter Topology.

4.2. Control Methods

The active control of a WPT system is predominantly focused on maximizing system efficiency and power transfer. Typically, the design considerations for active control of a static WPT system is focused on achieving fast and optimal operation when the system is first energized. Whereas dynamic, active control for WPT systems must consider a continuously varying mutual inductance throughout the operation and thus requires continuous feedback. The methods for this rely on understanding the system's state concerning the coupling coefficient/mutual inductance. A general approach for these measurements is found in [56,57].

Frequency tuning is among the most popular methods for the control of WPT systems. Resonance is a key factor in high-efficiency system operation. The resonant frequency can be determined for an inductor and capacitor combination is as follows:

$$f_0 = \frac{1}{2\pi\sqrt{L_p C_p}} \tag{17}$$

$$f_0 = \frac{1}{2\pi\sqrt{L_s C_s}} \tag{18}$$

where L_p and C_p, as seen in Figure 6, are the primary and secondary inductor and compensation capacitor. L_s and C_s are the respective secondary side inductor and compensation capacitor. When operating at the resonant frequency, the current and voltage through the components remain in phase. This means the compensating capacitor is effectively cancelling the phase shift effect of the inductor. In most cases, the goal of frequency tuning is

for a system to achieve or operate close to resonance quickly when power transfer begins or to maintain resonant operation under changing conditions. A change in mutual inductance affects power transfer and the suitability of components for operation. From [58], it is noted that systems with varying load conditions and changing distances between primary and secondary coils experience different efficiencies and output power when using a static operating frequency. Frequency tuning can be achieved through several methods, where the underlying concept is to probe the system to attain information about the power quality and/or power waveforms. This information is then applied to tune the frequency to a better match for system operation. In [59,60], by probing the primary side voltages and currents at specific parts of the system and using this information following the circuit's operating principles, the system's effectiveness can be found. The control systems then employ compensatory measures to adjust the frequency to get a more desirable operation. In some instances, it is not desirable to operate at the exact resonant frequency. By operating just outside the frequency, some circuits can avail of soft switching by leaving a small portion of the reactive effect on either the current or voltage waveforms in the system. Work in [61] highlights that with an LCL-S topology, the desired operating frequency lies just above that of the resonant one. This frequency tuning method has shown an efficiency improvement of up to 6% in some cases. This paper [61] bases its proposition on a technique where although the component values and resonant conditions were known, a perturb and observe method was used to achieve desired operation in a system that lacks such information. The importance of the quality factor is worth noting as it is an integral part of understanding system operation. A general maximum efficiency equation can be extrapolated from (16), where the total efficiency is the ratio of power dissipated across the load to total power dissipated as seen in (17):

$$\eta_s = \frac{I_2^2 R_{Le}}{I_1^2 R_1 + I_2^2 R_2 + I_2^2 R_{Le}} \tag{19}$$

Quality factor in RLC circuits such as the ones seen in WPT systems is a gauge of system behavior over a range of frequencies, where in a series circuit, the maximum current is achieved at resonance. However, in a parallel circuit, the minimum current is achieved at resonance. RLC circuits can operate as either purely resistive, inductive, or capacitive, depending on the operating frequency and circuit topology. The quality factor denoted by Q can be calculated using different approaches depending on what parameters are the focus of the investigation. Focusing on WPT with inductive coupling with the system depicted in Figure 1, Equations (18) and (19) are applicable:

$$Q_1 = \frac{\omega L_1}{R_1} \tag{20}$$

$$Q_2 = \frac{\omega L_2}{R_2} \tag{21}$$

where Q_1 and Q_2 denote the quality factor of the primary and secondary side coils, respectively. The voltage of the secondary can be denoted as:

$$U_2 = I_2^2(R_2 + R_L) = I_1 \omega M = I_1 \omega K \sqrt{L_1 L_2} \tag{22}$$

From (17)–(20) a general max efficiency can be extrapolated:

$$\eta_{max} = \frac{k^2 Q_1 Q_2}{\left(1 + \sqrt{1 + k^2 Q_1 Q_2}\right)^2} \tag{23}$$
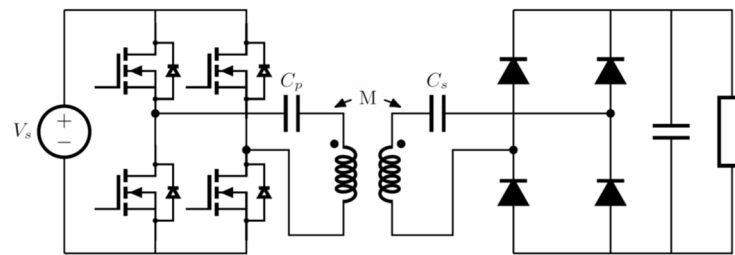
Figure 6. SS Compensated WPT System.

This general efficiency equation focuses on coil efficiency while ignoring losses in converters and compensation topologies. This highlights the importance of the quality factor in systems and shows system limitations.

In recent years research in frequency tunning has branched out to look at further possibilities for the control technique. As previously mentioned, a change in load condition and/or mutual inductance can change power output and efficiency. A phenomenon first mentioned in [14] known as bifurcation has been observed when subjecting systems to a varying mutual inductance. Bifurcation is the occurrence of "frequency splitting" where, at a specific coupling factor range, there are two instances of frequencies that are not resonant but still exhibit higher system efficiencies. Work in [62] highlights this phenomenon and presents a method of using one of the secondary frequencies as a means of delivering constant power and efficiency to a fixed load under a varying coupling coefficient. The study of WPT systems as two-port networks has gained notoriety in modern research. As seen in [17,63], viewing the system as a two-port network can present valuable insight into the desired operation and is especially useful in analyzing complex higher-order systems. Derivations for the two-port network analysis of a network can be found in [64]. A frequency tunning method in [65] proposes the objective of tuning via viewing the system as a matching network and focuses on the minimization of the reflection coefficient. The benefit of such a method is that whilst in the same coupling region as the bifurcation method when comparing the minimum reflection coefficient magnitude (MRCM) method to ZPA tuning, the MRCM method is reported to display greater power transfer and efficiency. Additionally, MRCM does not require information about the coupling factor or primary and secondary resonators.

Outside of frequency tuning, there are other inverter and switching related control methods. Phase shift control is a method of using switching to control the load resistance. The maximum power output can be obtained by matching the equivalent load to the conjugate output impedance ($Z_L = Z_0^*$) [66]. Phase shift control can achieve this via controlling the voltage output of the inverter/rectifier to change the equivalent load resistance, for which a control method can be seen in [67]. The work in [68] highlights that the condition ($Z_L = Z_0^*$) for maximum power transfer is generally not fulfilled at the same point of maximum efficiency which takes place at ($R_L = R_{L,opt}$, $X_L = -X_s$). It presents a means of overcoming this issue by controlling a DC-to-DC converter to vary the equivalent resistance of the load to achieve optimum efficiency for every value of output power. The concept of varying equivalent parameters for a passive component has been applied beyond just the load resistance. Within the last few years, research has been conducted into reactive power compensation via switch-controlled methods. Switch control methods first mentioned in [69] were proposed to control the equivalent inductance or capacitance of either the inductor or capacitor in a resonant circuit to modulate the resonant frequency to regulate the converters without a significant increase in switching losses. It is also stated that switch-controlled capacitors (SCC), seen in Figure 7, are better suited to higher frequency applications than switch-controlled inductors (SCI). When harmonics

higher than the second are neglected, then the equivalent inductance L_{sc} or capacitance C_{sc} can be determined by (24):

$$\frac{L_{sc}}{L_a} = \frac{C_{sc}}{C_a} = \frac{1}{2 - (2\alpha - sin2\alpha)/\pi} \tag{24}$$

where L_a and C_a are the actual inductance and capacitance of the components, and α denotes the phase shift between the voltage waveform across the SCI or SCC circuit and the switching driving signal.
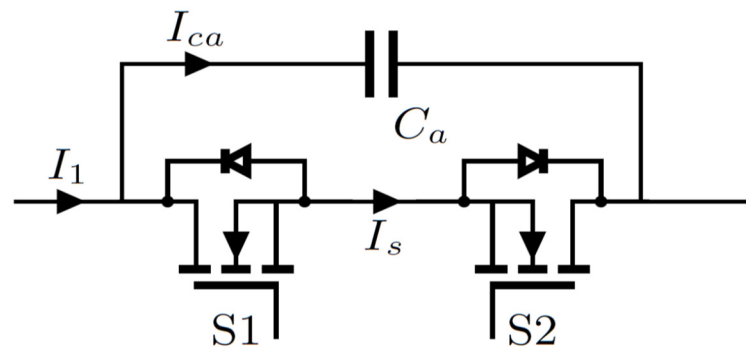

Figure 7. Switch Controlled Capacitor.

In [70,71], methods for utilizing SCC in WPT are presented to achieve reactive compensation to diminish frequency mismatch along with control for soft switching to increase system efficiency.

Another issue worth noting is the control for charging times in WPT systems. In plug-in electric vehicles (PEVs), the J1772A standard [72] outlined by the SAE details the use of a control pilot signal for the charger interface that relays information about the charging state of the EV. The control pilot signal is a pulse width modulated signal that is controlled by the EV and read by the charger. The J1772 control pilot is a 1 kHz $\pm$ 12 V square wave. The value of the voltage defines different state. The EV indicates its state via circuit resistance. The EV supply observes the voltage and modifies the state accordingly. The conditions for each state described in J1772 are summarized in Table 2 [72] and reflected in Figure 8.

Table 2. EV Control Pilot Signal States.

State	Pilot High	Pilot Low	Frequency	EV Resistance	Charging Status
State A	+12 V	N/A	DC	∞	Standby
State B	+9 $\pm$ 1 V	−12 V	1 kHz	2.74 kΩ	EV detected
State C	+6 $\pm$ 1 V	−12 V	1 kHz	882 Ω	EV ready (Charging)
State D	+3 $\pm$ 1 V	−12 V	1 kHz	246 Ω	Ventilation required
State E	0 V	0 V	N/A	N/A	No power
State F	N/A	−12 V	N/A	N/A	Error

Communications play a vital role in WPT for EV battery charging. The control techniques mentioned in this section rely on communications to send measurements and information from the vehicle to infrastructure (V2I) and vice versa. This can be achieved via two methods: to employ a stand-alone communications system and the second is to use the power waveform. The first method can be achieved by several means, including Bluetooth, Infrared and Near Field Connection (NFC). The system proposed by Oak Ridge National Laboratory (ORNL) in [73] uses a dedicated short-range communication (DSRC) link based on IEEE 802.11p Wi-Fi as a means of transmitting information from the secondary to the primary. The system employs dual Powerex Intellimod IGBTs in the H-bridge with a TMS320F28335 DSP module for control. The information from the secondary is

used to determine control measures for the system. An example of the second method of communication is explored in [38] which proposes a means of control for stationary EV charging by utilizing the power supply waveform. The method explains that a shunt path on the secondary side controlled by a switch to decouple the battery from the circuit can be used to reflect an impedance change to the primary. A protection circuit also accompanies this switching circuit to ensure the battery is not harmed. The waveform of the primary is continuously probed to learn the state of the system to determine whether to supply power to the transmitting coil. The most notable form of using the power waveform for communication is the Qi standard. The Qi standard is often adopted for low power devices, which modulates a 2 kHz signal within the power carrying waveform [74]. Methods such as this save on costly additional communications and allow for more compact systems.
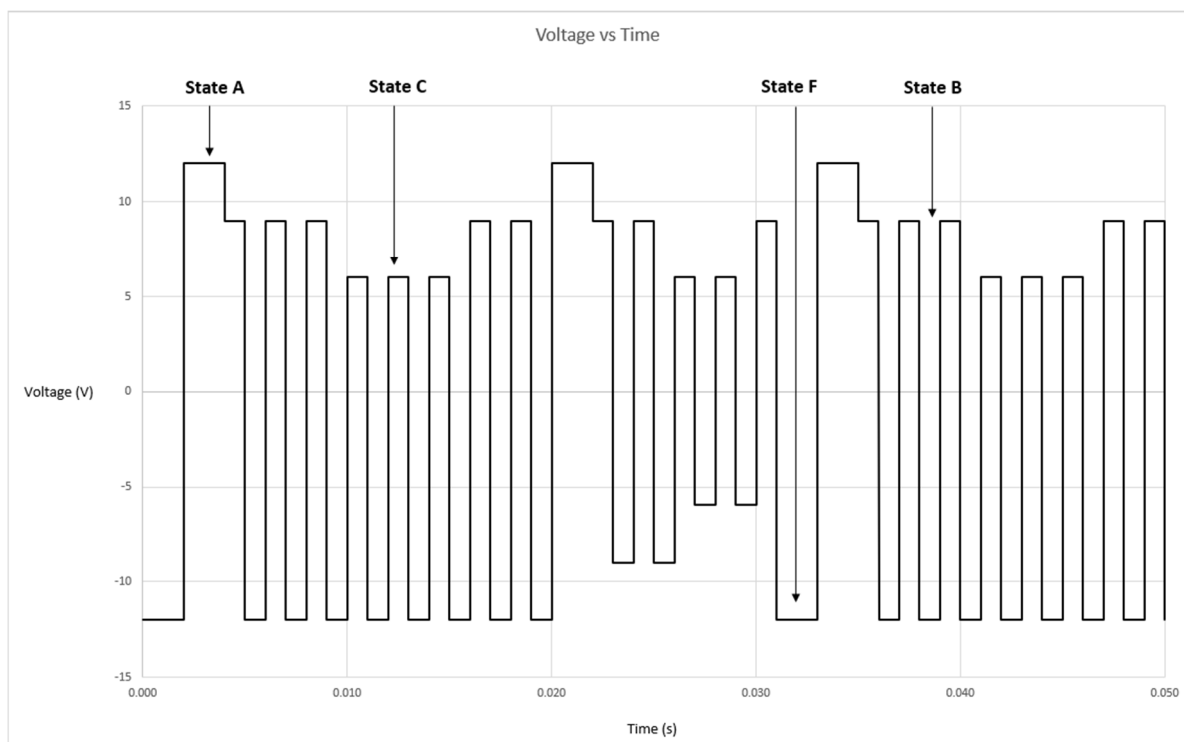

Figure 8. J1772 control pilot signal states.

5. Design Considerations

5.1. Coil Design

The coils of a WPT system are, in effect, the most critical aspect of the power transfer process. Without the coils, there is no conversion from electrical to magnetic waveforms and vice versa, enabling the transfer of power. As highlighted in Section 4, coil design plays an integral part in system performance. From Equation (21), it is shown that the quality factor of the coil is a key design consideration in overall system efficiency. This is also explored in [75]. For a stationary two-coil system, the coupling coefficient is around 0.2 with quality factors of approximately 300. This relates to a theoretical maximum power transfer efficiency of 96.7% [64]. The quality factor of the coils is related to the frequency bandwidth to which they are subjected too. Modern systems operate in the kHz range and due to the high frequency commonly used, Litz wire is the preferred winding as it shows reduced losses compared to traditional copper wire. As mentioned in various earlier sections, one of the most crucial factors in WPT systems is that of the coupling factor. The coupling factor of a system significantly affects the performance [76], and in the following subsections on stationary and dynamic charging, this design facet features prominently.

5.1.1. Stationary Charging

The basic coil shapes for WPT systems are depicted in Figure 9a,b. The traditional and most common coil referred to is the circular coil seen in Figure 9a. The refinement of design for circular coils can be found in [77,78]. The design of circular couplers is heavily influenced by the core. So far, the WPT system in this paper has been referred to as operating with an air core. This may not always be strictly true as, for many cases, systems have adapted to the use of ferrite in coil structures to guide magnetic flux. As seen in Figure 9, the ferrite sits behind the coil. It also, in many cases, is accompanied by a further aluminum backplate that acts as a shield to electromagnetic field (EMF) leakage. The use of ferrite also contributes to the inductance of the coil, changing the quality factor. The work in [79] explores the effects of ferrite and aluminum for different coil topologies. From [76], it is found that the optimum design for a circular pad using ferrite as seen in Figure 9a is satisfied by:

$$x = \frac{r_2}{r_4}, r_2 = \frac{r_1 + r_3}{2} \tag{25}$$

where r_1 is the distance from the centre of the pad to the inner circumference of the winding, r_2 is the distance from the centre of the pad to the middle of the winding, r_3 is the distance from the centre of the pad to the outer circumference of the winding and r_4 is the radius of the ferrite pad. x, in this case, is used in a larger equation to find the magnetic flux generated from the transmitting coil to a zero current secondary coil. It appears in the equation as $x^2(1 - x^2)$ where this factor should be maximized. By using differentiation, the maximum point for x, in this case, is 0.707. Primary circular coils are useful as they have omnidirectional characteristics and are simple to manufacture, but in recent years innovation in coil design has led to some significant breakthroughs. In 2010 the flat solenoid coupler (FSC) structure depicted in Figure 9f was introduced in [80]. This structure showed improved coupling factor, lateral misalignment tolerance and a short winding cable, reducing losses. Whilst this structure has benefits, it suffers from large electromagnetic field (EMF) radiation. The system generated flux on both sides of the pad, meaning potential coupling with other conductors lowering efficiency and induction heating of car chassis, which meant the system would need significant shielding. The cons outweighed the pros for most cases in EV charging, and a single-sided flux path was needed. The DD pad presented in [76] and shown in Figure 9c offered such a solution. The DD pad boasts a five times greater charging area than the circular design with similar material costs, improved lateral tolerance and the ability to transfer power at 200 mm. To further increase the misalignment resilience of DD pads, an additional quadrature coil named the Q coil is introduced in [81] to the topology resulting in the DDQ pad shown in Figure 9e. In [82], a bipolar receiver pad was tested against a DDQ receiver when subjected to DD and circular pad transmitters. It was found that a DDQ receiver over a DD pad offered a five times greater charging zone than that of the DDQ receiver over a circular transmitter. This paper also proposes a variant of the DD pad known as the bipolar pad (BPP) depicted in Figure 9d. BPP pads differ in design from DD pads as they have larger D windings that overlap one another. BPP shows similar characteristics to the DDQ but with the added benefit of using approximately 25% less copper. The work in [12] explores the resilience of DD and bipolar pads to horizontal misalignment in the range of ±300 mm, showing that systems can maintain coupling factors from 0.18–0.31. They also showed an ability to transfer 8 kW of power at air gaps of 200 mm with an efficiency of 95%. A more recent comparative study on the planar square coupler (PSC) against the FSC was also conducted in [83], showing that PSC exhibits desirable qualities from FSC, such as an independent self-inductance in relation to coupling factor and a moderate misalignment tolerance. PSC, which can be seen in Figure 9b, has the added benefit of not suffering from such a significant leakage inductance issue. As coil design is one of the most heavily researched areas in WPT for EV battery charging it is constantly evolving. In the past five years, there have been many new novel avenues explored within the technology. One such issue present in previously mentioned designs is that of null zones. Null zones refer to

zones of low magnetic coupling when systems are subject to misalignment. This is explored in [84], where it is stated that null zones for topologies such as circular and DD pads are at 40% and 35% of pad diameter and length, respectively. [82] proposes a Quadruple D-pad that boasts a single-sided flux with low leakage and losses with the added benefit of having no null zone. In 2019 a topology presented in [85] named the Tachi coil shows a new configuration that exhibits high misalignment tolerance. In general, the transfer efficiency is like that of circular and DD coils but, when subject to misalignment, presents a high coupling factor and flux linkage. Reconfigurable and multi coils systems have also been designed to change coil structure to suit misalignment. In [86], a reconfigurable topology is presented. The technology focuses on impedance matching to maximize power transfer with varying receiver distances. This is achieved by the introduction of an adjustable repeater coil. The adjustable repeater coil allows the system to change its input impedance to match the source impedance when the system is subject to varying receiver distances. The system boasts an improved transfer efficiency that allows for tunning of the coupling coefficient and quality factor. The work in [87] details a system with one additional coil on both the primary and secondary sides of the system. The four-coil system allows for constant current on the primary side and limits the increase in primary-side current when the secondary is not present. The system shows a less than 5% deviation when presented with varying loads between 40–60 Ω and maximum efficiency of 96.3% in well-aligned cases.
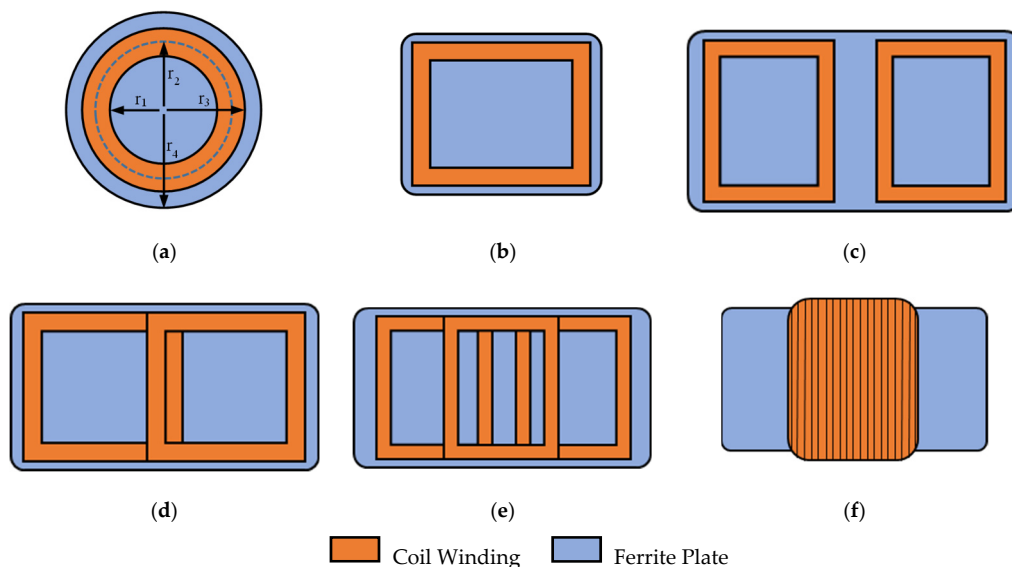

Figure 9. Coil Structures of WPT Systems for EV Battery Charging Including Ferrite Back-Plates. (**a**) Circular Coil. (**b**) Planar Square Coil. (**c**) DD Coil. (**d**) Bi-Polar Pad. (**e**) DDQ Coil. (**f**) Solenoid Coil.

5.1.2. Dynamic Charging

To continuously charge a moving load such as an RPEV or OLEV, dynamic battery charging has quite a different set-up to that of static charging. There are two main topologies of powered track in this form of charging. The first is a continuous track depicted in [10,36,88], where the inductive track flows continuously through the powered driving surface. There are several designs of a continuous track. The most basic track explored in [89] consists of two conductors accompanied by ferrite on the outside and between the conductors to guide flux, known as the W-type track. The next most common type of continuous track is the I-type which was proposed in [90]. Both the W-type and I-type tracks can be seen in Figure 10. For the W-type track, the distribution area of the ferrite determines the power transfer distance. The track should be designed so that the width of the track is four times greater than the distance of the pickup coil from the transmitter. The I-type, on the other hand, has no relation between track width and pickup height. The width between poles is chosen to maximize coupling, and the track width is chosen to

give desired lateral tolerance. Continuous tracks, whilst simple in design, come with some inherent issues. The problem of low coupling due to the pickup only covering a small part of the track at any time creates issues with efficiency and electromagnetic interference (EMI). To combat this, a segmented track is explored in [91,92] to reduce the EMI issue. The segment track is controlled only to be excited when an EV passes over it and shows the ability to drive several RPEVs selectively. Whilst the efficiency of the track is still below that of static charging at about 70–80%, the benefits of continual charging may outweigh the cons. This segmented approach is like the second kind of topology commonly found in dynamic charging. Intermittent coils explored in [93] can further reduce the EMI issue but require extensive control to operate with suitable efficiency. In [94], a variant of the DD coil is proposed to solve the issues of extremely low mutual inductance between intermittent coils in dynamic charging. The crossed DD topology is used with LCC compensation to realize a constant current with slow and smooth inductance variation. The pickup coils for dynamic wireless power transfer are the same as the coils seen in static charging. The work in [95] points to multi-thread coils being the most effective design for dynamic charging as they have advantages in misalignment tolerance and heating dissipation. A comparison of the coil designs detailed in this section is in Table 3.
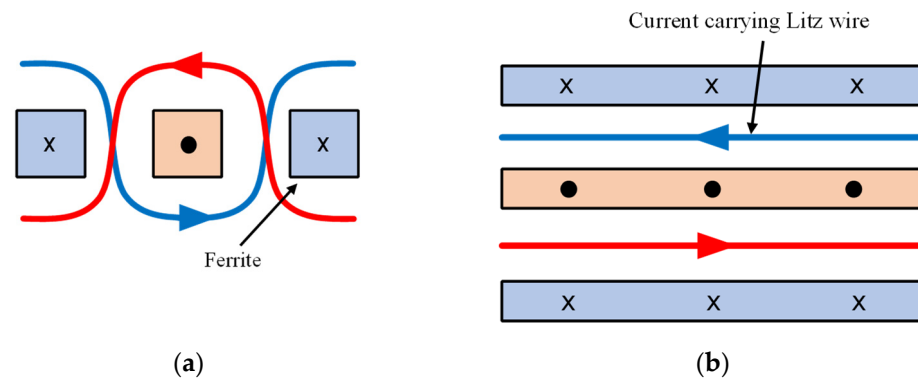

Figure 10. (**a**) I-Type and (**b**) W-Type Dynamic Track.

5.2. Safety Standards

In the early conception of modern WPT for EV battery charging, one of the main pushing points for the technology was safety. The SAE had proposed an inductive coupler in the late 1990s, focusing on safe charging in challenging weather conditions so users were not at risk of encountering exposed high-power conductors [96]. As the design changed over time to accommodate for large air gaps and focus more on the ergonomics of the system, safety concerns began to arise. In Section 5 of this paper, it is mentioned, there is an issue of EMI present in modern systems. In many cases, aluminum shielding is employed in coil design to reduce EMI. Also mentioned in Section 5 is ferrite back plating which is employed to control the flux path and reduce unwanted coupling to other devices and infrastructure. Due to the chassis of a car typically being made of steel, the onboard passengers using a WPT system to charge their EV are well protected against any radiation. In terms of human protection, the concern is for people(s) in close proximity outside of the vehicle. The International Commission on Non-Ionizing Radiation Protection (ICNIRP) is often looked to for guidance in this case. At the dawn of modern systems, the INCIRP released a standard in 1998 detailing a limit for public exposure to magnetic field strength for different bandwidths of charging frequency. After ten years of advancements and study, in 2010 the INCIRP changed their standards to reflect a new understanding of the topic. The 2010 guidelines on varying frequencies from 1 kHz to 100 kHz are outlined in [97], and the 2009 guidelines for static frequencies between 0 Hz–100 kHz are outlined in [98]. As WPT for EV battery charging is proposed to operate from 79–90 kHz, these guidelines apply. It is stated that for the public, a system with varying magnetic fields, such as is present in WPT. Exposure should be limited to 27 μT (where T = Tesla, Unit for Magnetic

Flux/Magnetic Field Strength). For occupational exposure, the limit is set at 100 μT. The SAE also released the j2954 standard [37] and proposed guidelines for interoperability, EMF, Safety testing and defined charging levels based on similar ones seen in the J1772 standard.

Table 3. Coil Functionality and Comparison.

Coil Type	Misalignment Tolerance	EMI & EMF	When to Use
Circular	Consistent through various orientations but suffers from null zones and limited range.	Back plate allows for shielding and single sided flux path.	Omnidirectional characteristics allows smooth operation for cases in which the EV may approach the coil from various angles.
FSC	Allows for high coupling factor and good tolerance for lateral displacement.	High EMI & EMF.	Operation over considerable air gaps.
DD	Somewhat stable charging over a significant area within and beyond the perimeter of the pad. Suffers from null zones.	Back plate allows for shielding and single sided flux path.	Effective for situations with low misalignment.
DDQ	Further increase in misalignment tolerance over DD pad.	Back plate allows for shielding and single sided flux path.	Offers a large charging area when over a DD pad. Good for situations with high misalignment.
BPP	Like that of DDQ.	Back plate allows for shielding and single sided flux path.	Reduction in material costs means it is a great alternative to DDQ pads.

5.3. Infrastructure and Cost

EV technology, as all emerging technology, is constantly scrutinized for the cost to performance ratio. For over 100 years, the technology has been stifled by the limitations and excessive costs of the battery. With modern EV batteries costing several hundred £/kWh and standard battery capacity being 40 kWh+ (Based on a Nissan Leaf [99]), the proportion in which the battery increases the price of an EV is readily apparent. As mentioned, WPT has been shown to reduce the battery size needed, which in turn could significantly decrease EV prices—but what are the costs for WPT systems? It is hard to determine as the technology is relatively new, and many systems differ in their chosen approach. The more costly option in WPT is dynamic charging, as it incurs not only the cost of the system but also high installation costs. In [100], the cost of installing both a W-type and I-type track is detailed. It shows a total cost of $1.07 million/km and $0.85 million/km, respectively. In [101], the estimate is as much as $2.4 million/lane/mile. Considering the length of suitable roadway in developed countries (in [101], it is stated that there are 2.6 million miles of paved roadways in the USA), the cost alone for total electrification is staggering. However, with the use of OLEVs, not every road would need to be upgraded as the EV would still have a means of propulsion outside of the powered roadways. It is stated in [102] that if 1% of urban roadways were powered, most vehicles could meet the 300 miles per charge target that matches standard ICE vehicles. Due to the cost and raw materials needed, dynamic charging may never be rolled out universally. However, there is still a compelling case for the technology. If implemented properly, the technology could see the unlimited range for EVs within city areas and possibly inter-city connections. Stationary EV charging is a different matter. The role of stationary charging is to make charging easier and safer. A 3.3 kW system akin to level 1 charging from Plugless Power can cost around $2000 [103]. This is a considerable cost increase from standard PEV chargers, but

the technology is only starting to be commercialized, and as demand grows, it would be expected to become more competitive. In general, the issue with the commercialization of EVs and their associated technologies have been in a catch-22 situation for decades. The uptake of EVs is needed as an incentive to build more infrastructure and charging products, but in the same vein, it is the infrastructure and products that need to become more widely available to allow for greater uptake in EVs. With government legislation and growing interest in technology, the rate of electrification will hopefully increase.

6. Discussion

WPT technologies' biggest competitor is standard wired charging, which is currently the most practical and dominant option. Within the last decade, there has also been the emergence of another solution to extend the EV range. Battery swapping stations explored in [104] are a new method for curbing range anxiety with EV users. The principle of the technology is to have a service station that swaps the spent battery of an EV amid its journey for a fully charged one from the station's stock. The empty battery is then recharged at the station, and the process is repeated. This functionally eliminates long charge wait times for EVs and, with planning, could make a long-range journey as seamless as that of using an ICE vehicle for the same purpose. This was trialed by a few companies, but it did not gain much traction. Scalability is a problem for this technology as, in theory, it requires a surplus of batteries in circulation so that there is no significant backlog of users waiting on charged batteries. It also requires expensive service stations, and interoperability for battery types and capacity would prove difficult.

To understand the advancement and scope of WPT for EV battery charging a chronological timeline is included below.

The information presented in Table 4 gives an overall impression of the developments and key areas of interest amongst researchers from the conception of the technology to the present. It is apparent that overall concerns with systems changed as new developments were made. In the early pre-2000's the focus was to validate that through magnetic coupling, substantial power could be transmitted. When this theory proved correct, a more practical mindset was adopted which is seen through the attention of the SAE and consideration towards the application of the technology. In the first decade of the 2000s research heavily focused on maintaining resonant operation to ensure good efficiency. This was principally achieved by studying compensation topologies and resulted in a new area of interest, namely, constant current and constant voltage. The realization that it may be possible to ensure suitable charging parameters for an EV from passive components put compensation design at the forefront of interest. However, in 2010 a more fundamental area of the technology regained notoriety. Coil design benefited from the increased power of general computing since the early 1990s. Whilst even in the earliest design [6] the coupled inductors are seen with ferrite moldings used to direct flux, new software packages and fast general computing allowed for researchers to produce more compact and detailed solutions. Better realization of magnetic flux paths meant designs with improved coupling factors meant the large air gap problem was slowly being overcome. At this point in the story of WPT for EV battery charging it is apparent that the overall system can be treated as a cascade of sub systems. Frequency tuning, compensation and coil design all present their own unique and vast challenges. In the middle of the 2010's, reaching closer to the current day, research around compensation and frequency tuning began to shift focus. Concern was now being paid to the power electronics in the form of wanting soft switching to increase efficiency. Compensation designs were now becoming increasingly complex as higher-order topologies were being explored. The goal for WPT systems that formed the middle of the 2010s remains almost identical today. From Table 4, it can be stated that a desired system exhibits the ability to provide a constant fixed voltage to the load for charging along with constant resonant operation and ZVS for maximum efficiency. In fact, a system of this specification could be achieved with a double LCC topology with input voltage control from a Buck-Boost converter. New coils only served to make this easier as

design is now focusing on steady and high coupling factors for misalignment. As stated in Section 4 an area that has remained mostly unchanged from early systems is the overall converter architecture. There have been some attempts at modifying the power electronics to streamline the system seen in [42,44,45] but the area is still lacking.

Table 4. WPT Advancement Timeline.

Period	Year	Example	Summary
1990–1995	1990	[6]	The first instance of modern dynamic WPT design where coupled inductors are used.
	1994	[7]	High frequnecy (10 kHz) employed to transfer kilowatts of power. Introduction of power electronics to drive the system.
1995–2001	1997	[96]	SAE shows interest in WPT for safe delivery of power to an EV.
	2000	[8]	Early consideration for practical application of WPT in a people mover system.
	2001	[36]	A review of challenges faced in WPT for EV battery charging. Disucssing resonance and quality factor.
2002–2007	2004	[14]	Further investigation into resonance and quality factor in relation to varying system frequency.
	2005	[88]	Investigates issues arising from varying coupling factor and phase shift.
	2005	[22]	Preposes a high-order compensation (LCL) network for WPT. Emphasises importance on desirable traits, such as CC and CV at resonance.
2007–2012	2009	[33]	Showcases a new frequency tuning method for LCL compensation networks.
	2009	[98]	ICNIRP guidelines on static frequencies.
	2010	[97]	ICNIRP guidelines on varying frequencies.
	2010	[80]	A revisiting of the coupler design to improve performance by better directing the magnetic flux.
	2011	[81]	Introduction of BPP to further improve coupling factor and mislagnment tolerance.
	2011	[11]	Full OLEV system constructed for testing.
	2012	[60]	Frequency tunning used to mitigate misalignment issues with standard circular coils.
	2012	[42]	A direct AC-AC converter system, this is one of the first preposals for streamlining the system.

Table 4. *Cont.*

Period	Year	Example	Summary
2013–2018	2013	[76]	Further research in the DD pad.
	2013	[44]	Introduction of Class E^2 converters for WPT, showcases a heavily streamlined system.
	2013	[91]	Further design consideration for OLEV supply side.
	2014	[12]	Further design improvments to BPP with the system able to tranfer power across 200 mm airgap.
	2015	[21]	An investigatioin into power supply types combined with the basic compensation topologies.
	2015	[18]	Preposes using switching to avail of mutliple compensation topolgies in a single system.
	2015	[25]	A comprehensive design for LCC compensation showcasing operation with ZVS and a constant resonance.
	2016	[23]	Inverstigation into double the LCL network showcasing CC & ZVS operation.
	2016	[48]	First instance of preposing split capacitor with sinlge switch converter topologies. Presents a new P5 buck-boost topolgy with reduced split capacitor size.
	2017	[17]	A comprehensive inverstigation into higher-order compensation to find desirable operation.
	2017	[38]	Preposes a method for control of the primary power output in relation to battery charge without wireless communications.
	2017	[45]	Further analysis on class E^2 converters for WPT.
	2018	[16]	Employing a controller to gain CC/CV operation from basic compensation topolgies.
2019–2022	2019	[71]	A switch controlled capacitor is used to maintain resonant operation.
	2019	[46]	ZVS for class E inverter over varying coupling factor.
	2019	[51]	The first instance of single switched Buck-Boost converts considered as full WPT systems.
	2019	[85]	New coil for misalignment tolerance to ensure a consistant power supply to the secondary.
	2019	[86]	Preposes a system that uses a switch controller capacitor bank to compensate for air gap variation.
	2019	[34]	Multi-load WPT system resiliant to changes in load.
	2020	[70]	Further reseatch into switch controller capacitors for resonance issues.
	2020	[54]	Introduction of Bi-directionality for vehicle to grid purposes.
	2020	[31]	Utilises the 3rd harmonic in conjuction with a modifcation of the basic compensation topologies to increase stability over varying coupling factor.
	2020	[57]	Showcases an impedance matching network that can be tuned to maximize efficiency over varying coupling factors.
	2021	[61]	Preposes using variable freuqnecy to ensure good effiency and CV operation for the load.

7. Conclusions

In this article, a comprehensive review of the WPT systems for electric battery charging focusing on inductive power transfer is presented. The basic WPT principles of electric battery charging is investigated. The compensation topologies are compared, including quality factor, reflected resistance, primary capacitance, primary current, resonance and operation capabilities. Power electronics converter topologies are detailed to give an understanding of the driving mechanisms within the system. The paper also addresses coil design, infrastructure, cost and safety standards. WPT for EV battery charging offers an ergonomic means of tackling the range and charge time anxieties surrounding EVs. Every year research pushes the technology further, and with the emergence of commercial units, the technology is about to gain its foothold. Whilst the advancements in recent years have been significant. There are still important challenges to overcome. One such issue is that WPT systems require more converter stages than their plug-in counterparts. Since the conception of the modern WPT system, the overall basic topology has remained undisturbed. Typically, even the most modern systems rely on the same power electronics set-up, which can be costly and require significant onboard space. This paper details many advancements in system topologies and operation. A revisiting of the power electronics in WPT for EV battery charging could be highly beneficial in increasing the commercial ability of the technology. One such area that has not been widely explored is DC-DC converter topologies as full WPT systems. As mentioned in Section 4, research has shown that split capacitor DC-DC converter topologies exhibit desirable traits for WPT with an overall reduction in converter stages and switches. It is stated in the literature that the current Buck-Boost systems struggle when operating over a limited/small magnetizing inductance. The isolated Cuk and P5 converters mentioned in Section 4 both use a high frequency transformer which has a large magnetizing inductance; this allows the system to maintain its Buck-Boost characteristic. For the case of WPT for EV battery charging, the mutual inductance would equate to the magnetizing inductance. This means the magnetizing inductance of a WPT system is far smaller than that of a ferrite core transformer. Thus, the Buck-Boost characteristic may not be maintained in this scenario with current designs. However, if the Buck-Boost characteristic can be maintained then a significant reduction in the needed converter stages can be realized for WPT systems. This system would eliminate the need for up to four of the converter stages, reducing the system to only 2, which is in-line with the standard plug-in systems. It would also allow for built in control of the output voltage via duty cycle control, ensuring a consistent 400 V that is needed for EV battery charging. The system may also avail of a reduction in the necessary communications needed for control of the output. If the input voltage and current are known along with the duty cycle, there is then an expected output. Thus, the system could operate with single side control, needing only information from the power transmitting side. This innovative technology looks as promising as the class E^2 converter, which is a similar technology that is gaining traction for use in WPT systems. Further research is needed into the application of these Buck-Boost converters in the context of wireless EV battery charging.

Conflicts of Interest: The authors declare no conflict of interest. The funders had no role in the design of the study; in the collection, analyses, or interpretation of data; in the writing of the manuscript, or in the decision to publish the results.

References

1. Yang, C. Running battery electric vehicles with extended range: Coupling cost and energy analysis. *Appl. Energy* **2021**, *306*, 118116. [CrossRef]
2. Cano, Z.P.; Banham, D.; Ye, S. Batteries and fuel cells for emerging electric vehicle markets Optimal storage and renewable distributed energy resources planning in distribution network View project Battery Pack Testing and Modeling View project. *Nat. Energy* **2018**, *3*, 279–289. [CrossRef]
3. Tu, H.; Feng, H.; Srdic, S.; Lukic, S. Extreme Fast Charging of Electric Vehicles: A Technology Overview. *IEEE Trans. Transp. Electrif.* **2019**, *5*, 861–878. [CrossRef]
4. Hutin, M.; Leblanc, M. Transformer System for Electric Rails-Ways. U.S. Patent 23 October 1894. Available online: https://patents.google.com/patent/US527857A/en (accessed on 26 January 2021).
5. Shladover, S.E. The Roadway-Powered Electric Transit Vehicle-Progress and Prospects. 1986. Available online: http://onlinepubs .trb.org/Onlinepubs/trr/1987/1155/1155-004.pdf (accessed on 2 February 2021).
6. Eghtesadi, M. Inductive power transfer to an electric vehicle-analytical model. In Proceedings of the IEEE Vehicular Technology Conference, Orlando, FL, USA, 6–9 May 1990; pp. 100–104. [CrossRef]
7. Green, A.W.; Boys, J.T. 10 kHz inductively coupled power transfer—concept and control. In Proceedings of the IEEE Conference Publication, London, UK, 26–28 October 1994; Volume 399, pp. 694–699. [CrossRef]
8. Covic, G.A.; Elliott, G.; Stielau, O.H.; Green, R.M.; Boys, J.T. The design of a contact-less energy transfer system for a people mover system. In Proceedings of the PowerCon 2000—2000 International Conference on Power System Technology, Perth, WA, Australia, 4–7 December 2000; Volume 1, pp. 79–84. [CrossRef]
9. Boys, J.T.; Elliott, G.A.J.; Covic, G.A. An appropriate magnetic coupling co-efficient for the design and comparison of ICPT pickups. *IEEE Trans. Power Electron.* **2007**, *22*, 333–335. [CrossRef]
10. Boys, J.T.; Huang, C.Y.; Covic, G.A. Single-phase unity power-factor inductive power transfer system. In Proceedings of the PESC Record—IEEE Annual Power Electronics Specialists Conference, Rhodes, Greece, 15–19 June 2008; pp. 3701–3706. [CrossRef]
11. Suh, N.P.; Cho, D.H.; Rim, C.T. Design of online electric vehicle (OLEV). In Proceedings of the Global Product Development—Proceedings of the 20th CIRP Design Conference, Nantes, France, 19–21 April 2010; pp. 3–8. [CrossRef]
12. Nguyen, T.D.; Li, S.; Li, W.; Mi, C.C. Feasibility study on bipolar pads for efficient wireless power chargers. In Proceedings of the Conference Proceedings—IEEE Applied Power Electronics Conference and Exposition—APEC, Fort Worth, TX, USA, 16–20 March 2014; pp. 1676–1682. [CrossRef]
13. Harris, S.T. *Circuit Analysis II with MATLAB Computing and Simulink/SimPowerSystems Modeling*; Orchard Publications: Fermont, QC, Canada, 2009.
14. Wang, C.S.; Covic, G.A.; Stielau, O.H. Power Transfer Capability and Bifurcation Phenomena of Loosely Coupled Inductive Power Transfer Systems. *IEEE Trans. Ind. Electron.* **2004**, *51*, 148–157. [CrossRef]
15. Bi, Z.; Kan, T.; Mi, C.C.; Zhang, Y.; Zhao, Z.; Keoleian, G.A. A review of wireless power transfer for electric vehicles: Prospects to enhance sustainable mobility. *Appl. Energy* **2016**, *179*, 413–425. [CrossRef]
16. Song, K.; Li, Z.; Jiang, J.; Zhu, C. Constant Current/Voltage Charging Operation for Series-Series and Series-Parallel Compensated Wireless Power Transfer Systems Employing Primary-Side Controller. *IEEE Trans. Power Electron.* **2018**, *33*, 8065–8080. [CrossRef]
17. Qu, X.; Jing, Y.; Han, H.; Wong, S.C.; Tse, C.K. Higher Order Compensation for Inductive-Power-Transfer Converters with Constant-Voltage or Constant-Current Output Combating Transformer Parameter Constraints. *IEEE Trans. Power Electron.* **2017**, *32*, 394–405. [CrossRef]
18. Qu, X.; Han, H.; Wong, S.C.; Tse, C.K.; Chen, W. Hybrid IPT Topologies with Constant Current or Constant Voltage Output for Battery Charging Applications. *IEEE Trans. Power Electron.* **2015**, *30*, 6329–6337. [CrossRef]
19. Villa, J.L.; Sallán, J.; Osorio, J.F.S.; Llombart, A. High-misalignment tolerant compensation topology for ICPT systems. *IEEE Trans. Ind. Electron.* **2012**, *59*, 945–951. [CrossRef]
20. Zhang, W.; Wong, S.C.; Tse, C.K.; Chen, Q. Design for efficiency optimization and voltage controllability of series-series compensated inductive power transfer systems. *IEEE Trans. Power Electron.* **2014**, *29*, 191–200. [CrossRef]
21. Sohn, Y.H.; Choi, B.H.; Lee, E.S.; Lim, G.C.; Cho, G.H.; Rim, C.T. General Unified Analyses of Two-Capacitor Inductive Power Transfer Systems: Equivalence of Current-Source SS and SP Compensations. *IEEE Trans. Power Electron.* **2015**, *30*, 6030–6045. [CrossRef]
22. Borage, M.; Tiwari, S.; Kotaiah, S. Analysis and design of an LCL-T resonant converter as a constant-current power supply. *IEEE Trans. Ind. Electron.* **2005**, *52*, 1547–1554. [CrossRef]
23. Liu, C.; Ge, S.; Guo, Y.; Li, H.; Cai, G. Double-lcl resonant compensation network for electric vehicles wireless power transfer: Experimental study and analysis. *IET Power Electron.* **2016**, *9*, 2262–2270. [CrossRef]
24. Yao, Y.; Wang, Y.; Liu, X.; Lin, F.; Xu, D. A Novel Parameter Tuning Method for a Double-Sided LCL Compensated WPT System with Better Comprehensive Performance. *IEEE Trans. Power Electron.* **2018**, *33*, 8525–8536. [CrossRef]
25. Li, S.; Li, W.; Deng, J.; Nguyen, D.; Mi, C.C. A Double-Sided LCC Compensation Network and Its Tuning Method for Wireless Power Transfer. *IEEE Trans. Veh. Technol.* **2015**, *64*, 2261–2273. [CrossRef]
26. Li, W.; Zhao, H.; Deng, J.; Li, S.; Mi, C.C. Comparison Study on SS and double-sided LCC compensation topologies for EV/PHEV Wireless Chargers. *IEEE Trans. Veh. Technol.* **2016**, *65*, 4429–4439. [CrossRef]

27. Li, W.; Zhao, H.; Li, S.; Deng, J.; Kan, T.; Mi, C.C. Integrated LCC Compensation Topology for Wireless Charger in Electric and Plug-in Electric Vehicles. *IEEE Trans. Ind. Electron.* **2015**, *62*, 4215–4225. [CrossRef]

28. Kan, T.; Nguyen, T.D.; White, J.C.; Malhan, R.K.; Mi, C.C. A new integration method for an electric vehicle wireless charging system using LCC compensation topology: Analysis and design. *IEEE Trans. Power Electron.* **2017**, *32*, 1638–1650. [CrossRef]

29. Nguyen, V.T.; Yu, S.D.; Yim, S.W.; Park, K. Optimizing compensation topologies for inductive power transfer at different mutual inductances. In Proceedings of the 2017 IEEE PELS Workshop on Emerging Technologies: Wireless Power Transfer, WoW, Chongqing, China, 20–22 May 2017; pp. 153–156. [CrossRef]

30. Zhang, X.; Wang, J.; Xue, M.; Li, Y.; Yang, Q. Reserch on Dynamic Wireless Charging of Electric Vehicle Based on Double LCC Compensation Mode. In Proceedings of the 2019 IEEE Wireless Power Transfer Conference, WPTC 2019, London, UK, 18–21 June 2019; pp. 141–145. [CrossRef]

31. Liu, Z.; Su, M.; Zhu, Q.; Zhao, L.; Hu, P. A Dual Frequency Tuning Method for Improved Coupling Tolerance of Wireless Power Transfer System. *IEEE Trans. Power Electron.* **2020**, *36*, 7360–7365. [CrossRef]

32. DigitalCommons, U.; Wu, H.H. Aaron Gilchrist Ky Sealy Daniel Bronson. A High Efficiency 5kW Inductive Charger for Evs using Dual Side Control. *IEEE Trans. Ind. Inform.* **2012**, *8*, 585–595. [CrossRef]

33. Kissin, M.L.G.; Huang, C.Y.; Covic, G.A.; Boys, J.T. Detection of the tuned point of a fixed-frequency LCL resonant power supply. *IEEE Trans. Power Electron.* **2009**, *24*, 1140–1143. [CrossRef]

34. Cheng, C.; Lu, F.; Zhou, Z.; Li, W.; Zhu, C.; Zhang, H.; Deng, Z.; Chen, X.; Mi, C.C. Load-independent wireless power transfer system for multiple loads over a long distance. *IEEE Trans. Power Electron.* **2019**, *34*, 9279–9288. [CrossRef]

35. Song, B.; Shin, J.; Lee, S.; Shin, S.; Kim, Y.; Jeon, S.; Jung, G. Design of a high power transfer pickup for Online Electric Vehicle (OLEV). In Proceedings of the 2012 IEEE International Electric Vehicle Conference, Greenville, SC, USA, 4–8 March 2012. [CrossRef]

36. Wang, C.S.; Covic, G.A.; Stielau, O.H. General stability criterions for zero phase angle controlled loosely coupled inductive power transfer systems. In Proceedings of the IECON Proceedings (Industrial Electronics Conference), Denver, CO, USA, 29 November–2 December 2001; Volume 2, pp. 1049–1054. [CrossRef]

37. J2954: Wireless Power Transfer for Light-Duty Plug-in/Electric Vehicles and Alignment Methodology—SAE International. Available online: https://www.sae.org/standards/content/j2954_202010/ (accessed on 12 March 2021).

38. Zhong, W.; Hui, S.Y.R. Charging Time Control of Wireless Power Transfer Systems Without Using Mutual Coupling Information and Wireless Communication System. *IEEE Trans. Ind. Electron.* **2017**, *64*, 228–235. [CrossRef]

39. Fu, M.; Ma, C.; Zhu, X. A cascaded boost-buck converter for high-efficiency wireless power transfer systems. *IEEE Trans. Ind. Inform.* **2014**, *10*, 1972–1980. [CrossRef]

40. Chinthavali, M.; Onar, O.C.; Campbell, S.L.; Tolbert, L.M. Isolated wired and wireless battery charger with integrated boost converter for PEV applications. In Proceedings of the 2015 IEEE Energy Conversion Congress and Exposition, ECCE 2015, Montreal, QC, Canada, 20–24 September 2015; pp. 607–614. [CrossRef]

41. Huang, Y.; Shinohara, N.; Mitani, T. Theoretical analysis on DC-DC converter for impedance matching of a rectifying circuit in wireless power transfer. In Proceedings of the 2015 IEEE International Symposium on Radio-Frequency Integration Technology, RFIT 2015—Proceedings, Sendai, Japan, 26–28 August 2015; pp. 229–231. [CrossRef]

42. Li, H.L.; Hu, A.P.; Covic, G.A. A direct AC-AC converter for inductive power-transfer systems. *IEEE Trans. Power Electron.* **2012**, *27*, 661–668. [CrossRef]

43. Chen, W.X.; Chen, Q.H. Application of class-E converter in magnetic resonant WPT system. In Proceedings of the AUS 2016—2016 IEEE/CSAA International Conference on Aircraft Utility Systems, Beijing, China, 10–12 October 2016; pp. 320–324. [CrossRef]

44. Nagashima, T.; Inoue, K.; Wei, X.; Bou, E.; Alarcon, E.; Sekiya, H. Inductively coupled wireless power transfer with class-E2 DC-DC converter. In Proceedings of the 2013 European Conference on Circuit Theory and Design (ECCTD), Dresden, Germany, 8–12 September 2013. [CrossRef]

45. Nagashima, T.; Wei, X.; Bou, E.; Alarcón, E.; Kazimierczuk, M.K.; Sekiya, H. Steady-State Analysis of Isolated Class-E2 Converter Outside Nominal Operation. *IEEE Trans. Ind. Electron.* **2017**, *64*, 3227–3238. [CrossRef]

46. Ayachit, A.; Corti, F.; Reatti, A.; Kazimierczuk, M.K. Zero-voltage switching operation of transformer class-E inverter at any coupling coefficient. *IEEE Trans. Ind. Electron.* **2019**, *66*, 1809–1819. [CrossRef]

47. Alhurayyis, I.; Elkhateb, A.; Morrow, D.J. Isolated and Non-Isolated DC-to-DC Converters for Medium Voltage DC Networks: A Review. *IEEE J. Emerg. Sel. Top. Power Electron.* **2020**, *9*, 7486–7500. [CrossRef]

48. Williams, B.W. Transformer Isolated Buck-Boost Converters. Available online: http://apc.aast.edu/ojs/index.php/RESD/article/viewFile/02.2.112/89 (accessed on 16 March 2021).

49. Elkhateb, A.; Rahim, N.A.; Selvaraj, J.; Williams, B.W. DC-to-DC Converter With Low Input Current Ripple for Maximum Photovoltaic Power Extraction. *IEEE Trans. Ind. Electron.* **2015**, *62*, 2246–2256. [CrossRef]

50. Elkhateb, A.; Rahim, N.A.; Selvaraj, J.; Uddin, M.N. Fuzzy-Logic-Controller-Based SEPIC Converter for Maximum Power Point Tracking. *IEEE Trans. Ind. Appl.* **2014**, *50*, 2349–2358. [CrossRef]

51. Elkhateb, A.; Adam, G.; Morrow, D.J. DC-to-DC Converter Topologies for Wireless Power Transfer in Electric Vehicles. In Proceedings of the IECON Proceedings (Industrial Electronics Conference), Lisbon, Portugal, 14–17 October 2019; Volume 2019, pp. 1665–1669. [CrossRef]

52.　Kezunovic, M. BEVs/PHEVs as dispersed energy storage in smart grid. In Proceedings of the 2012 IEEE PES Innovative Smart Grid Technologies, Washington, DC, USA, 16–20 January 2012. [CrossRef]

53.　Liu, C.; Chau, K.T.; Wu, D.; Gao, S. Opportunities and challenges of vehicle-to-home, vehicle-to-vehicle, and vehicle-to-grid technologies. *Proc. IEEE* **2013**, *101*, 2409–2427. [CrossRef]

54.　Onar, O.C.; Su, G.; Asa, E.; Pries, J.; Galigekere, V.; Seiber, L.; White, C.; Wiles, R.; Wilkins, J. 20-kW Bi-directional Wireless Power Transfer System with Energy Storage System Connectivity. In Proceedings of the Conference Proceedings—IEEE Applied Power Electronics Conference and Exposition—APEC, New Orleans, LA, USA, 15–19 March 2020; Volume 2020, pp. 3208–3214. [CrossRef]

55.　Pellitteri, F.; Boscaino, V.; di Tommaso, A.O.; Miceli, R. Efficiency optimization in bi-directional inductive power transfer systems. In Proceedings of the Electrical Systems for Aircraft, Railway and Ship Propulsion, ESARS, Aachen, Germany, 3–5 March 2015; Volume 2015. [CrossRef]

56.　Jiwariyavej, V.; Imura, T.; Hori, Y. Coupling coefficients estimation of wireless power transfer system via magnetic resonance coupling using information from either side of the system. *IEEE J. Emerg. Sel. Top. Power Electron.* **2015**, *3*, 191–200. [CrossRef]

57.　Liu, Y.; Feng, H. Maximum Efficiency Tracking Control Method for WPT System Based on Dynamic Coupling Coefficient Identification and Impedance Matching Network. *IEEE J. Emerg. Sel. Top. Power Electron.* **2020**, *8*, 3633–3643. [CrossRef]

58.　Cao, Y.; Qahouq, J.A.A. Evaluation of maximum system efficiency and maximum output power in two-coil wireless power transfer system by using modeling and experimental results. In Proceedings of the Conference Proceedings—IEEE Applied Power Electronics Conference and Exposition—APEC, Tampa, FL, USA, 26–30 March 2017; pp. 1625–1631. [CrossRef]

59.　Abramov, E.; Peretz, M.M. Adaptive Self-Tuned Mixed-Signal Controller IC for Resonant Wireless Power Transfer. In Proceedings of the Conference Proceedings—IEEE Applied Power Electronics Conference and Exposition—APEC, New Orleans, LA, USA, 15–19 March 2020; Volume 2020, pp. 805–812. [CrossRef]

60.　Krishnan, S.; Bhuyan, S.; Kumar, V.P.; Wang, W.; al Afif, J.; Lim, K.S. Frequency agile resonance-based wireless charging system for electric vehicles. In Proceedings of the 2012 IEEE International Electric Vehicle Conference, Greenville, SC, USA, 4–8 March 2012. [CrossRef]

61.　Babaki, A.; Vaez-Zadeh, S.; Zakerian, A.; Covic, G.A. Variable-Frequency Retuned WPT System for Power Transfer and Efficiency Improvement in Dynamic EV Charging with Fixed Voltage Characteristic. *IEEE Trans. Energy Convers.* **2021**, *36*, 2141–2151. [CrossRef]

62.　Mastri, F.; Costanzo, A.; Mongiardo, M. Coupling-Independent Wireless Power Transfer. *IEEE Microw. Wirel. Components Lett.* **2016**, *26*, 222–224. [CrossRef]

63.　Fathi, D.A.; Fouda, M.E.; Said, L.A.; Khafagy, N.R.; Radwan, A.G. Two-Port Network Analysis of Equal Fractional-order Wireless Power Transfer Circuit. In Proceedings of the International Conference on Microelectronics, ICM, Aqaba, Jordan, 14–17 December 2020; Volume 2020. [CrossRef]

64.　Li, S.; Mi, C.; Mi, C.C. 2014 JESTPE Li Siqi Application Wireless Power Transfer for Electric Vehicle Applications. *IEEE J. Emerg. Sel. Top. Power Electron.* **2015**, *3*, 4–17. [CrossRef]

65.　Seo, D.W.; Lee, J.H. Frequency-Tuning Method Using the Reflection Coefficient in a Wireless Power Transfer System. *IEEE Microw. Wirel. Components Lett.* **2017**, *27*, 959–961. [CrossRef]

66.　Kong, S.; Kim, M.; Koo, K.; Ahn, S.; Bae, B.; Kim, J. Analytical expressions for maximum transferred power in wireless power transfer systems. In Proceedings of the IEEE International Symposium on Electromagnetic Compatibility, Long Beach, CA, USA, 14–19 August 2011; pp. 379–383. [CrossRef]

67.　Zhao, C.; Wang, Z.; Du, J.; Wu, J.; Zong, S.; He, X. Active resonance wireless power transfer system using phase shift control strategy. In Proceedings of the Conference Proceedings—IEEE Applied Power Electronics Conference and Exposition—APEC, Fort Worth, TX, USA, 16–20 March 2014; pp. 1336–1341. [CrossRef]

68.　Berger, A.; Agostinelli, M.; Vesti, S.; Oliver, J.A.; Cobos, J.A.; Huemer, M. A Wireless Charging System Applying Phase-Shift and Amplitude Control to Maximize Efficiency and Extractable Power. *IEEE Trans. Power Electron.* **2015**, *30*, 6338–6348. [CrossRef]

69.　Gu, W.J.; Harada, K. A New Method to Regulate Resonant Converters. *IEEE Trans. Power Electron.* **1988**, *3*, 430–439. [CrossRef]

70.　Zhang, J.; Zhao, J.; Zhang, Y.; Deng, F. A Wireless Power Transfer System with Dual Switch-Controlled Capacitors for Efficiency Optimization. *IEEE Trans. Power Electron.* **2020**, *35*, 6091–6101. [CrossRef]

71.　Zhao, J.; Zhang, J.; Zhang, Y.; Din, Z.; Juri, J. A Reactive Compensation Method Using Switch Controlled Capacitor for Wireless Power Transfer. In Proceedings of the 2019 IEEE Energy Conversion Congress and Exposition, ECCE 2019, Baltimore, MD, USA, 29 September–3 October 2019; pp. 2112–2117. [CrossRef]

72.　J1772A: SAE Electric Vehicle and Plug in Hybrid Electric Vehicle Conductive Charge Coupler—SAE International. Available online: https://www.sae.org/standards/content/j1772_201710/ (accessed on 4 May 2021).

73.　Miller, J.M.; White, C.P.; Onar, O.C.; Ryan, P.M. Grid side regulation of wireless power charging of plug-in electric vehicles. In Proceedings of the 2012 IEEE Energy Conversion Congress and Exposition, ECCE 2012, Raleigh, NC, USA, 15–20 September 2012; pp. 261–268. [CrossRef]

74.　Van Wageningen, D.; Staring, T. The Qi wireless power standard. In Proceedings of the 14th International Power Electronics and Motion Control Conference EPE-PEMC 2010, Ohrid, Macedonia, 6–8 September 2010. [CrossRef]

75. Li, J.; Deng, Q.; Hu, W.; Zhou, H. Research on quality factor of the coils in wireless power transfer system based on magnetic coupling resonance. In Proceedings of the 2017 IEEE PELS Workshop on Emerging Technologies: Wireless Power Transfer, WoW 2017, Chongqing, China, 20–22 May 2017; pp. 123–127. [CrossRef]

76. Budhia, M.; Boys, J.T.; Covic, G.A.; Huang, C.Y. Development of a single-sided flux magnetic coupler for electric vehicle IPT charging systems. *IEEE Trans. Ind. Electron.* **2013**, *60*, 318–328. [CrossRef]

77. Budhia, M.; Covic, G.A.; Boys, J.T. Design and optimization of circular magnetic structures for lumped inductive power transfer systems. *IEEE Trans. Power Electron.* **2011**, *26*, 3096–3108. [CrossRef]

78. Rim, C.T.; Mi, C. *Wireless Power Transfer for Electric Vehicles and Mobile Devices*; John Wiley & Sons: Hoboken, NJ, USA, 2017.

79. Knaisch, K.; Springmann, M.; Gratzfeld, P. Comparison of coil topologies for inductive power transfer under the influence of ferrite and aluminum. In Proceedings of the 2016 Eleventh International Conference on Ecological Vehicles and Renewable Energies (EVER), Monte Carlo, Monaco, 6–8 April 2016. [CrossRef]

80. Budhia, M.; Covic, G.; Boys, J. A new IPT magnetic coupler for electric vehicle charging systems. In Proceedings of the IECON Proceedings (Industrial Electronics Conference), Glendale, AZ, USA, 7–10 November 2010; pp. 2487–2492. [CrossRef]

81. Covic, G.A.; Kissin, M.L.G.; Kacprzak, D.; Clausen, N.; Hao, H. A bipolar primary pad topology for EV stationary charging and highway power by inductive coupling. In Proceedings of the IEEE Energy Conversion Congress and Exposition: Energy Conversion Innovation for a Clean Energy Future, ECCE 2011, Phoenix, AZ, USA, 17–22 September 2011; pp. 1832–1838. [CrossRef]

82. Zaheer, A.; Kacprzak, D.; Covic, G.A. A bipolar receiver pad in a lumped IPT system for electric vehicle charging applications. In Proceedings of the 2012 IEEE Energy Conversion Congress and Exposition, ECCE 2012, Raleigh, NC, USA, 15–20 September 2012; pp. 283–290. [CrossRef]

83. Yao, Y.; Gao, S.; Wang, Y.; Zhang, S.; Liu, X.; Xu, D. A Comparison Study between Flat Solenoid Coupler and Planar Square Coupler for WPT Systems. In Proceedings of the IECON Proceedings (Industrial Electronics Conference), Lisbon, Portugal, 14–17 October 2019; Volume 2019, pp. 3431–3435. [CrossRef]

84. Ahmad, A.; Alam, M.S.; Mohamed, A.A.S. Design and Interoperability Analysis of Quadruple Pad Structure for Electric Vehicle Wireless Charging Application. *IEEE Trans. Transp. Electrif.* **2019**, *5*, 934–945. [CrossRef]

85. Li, Y.; Zhao, J.; Yang, Q.; Liu, L.; Ma, J.; Zhang, X. A Novel Coil with High Misalignment Tolerance for Wireless Power Transfer. *IEEE Trans. Magn.* **2019**, *55*, 1–4. [CrossRef]

86. Hu, J.; Lee, C.K.; Ho-Chinglu, H. Reconfigurable wireless power transfer systems for distance adaptation. In Proceedings of the Proceedings—IEEE International Symposium on Circuits and Systems, Sapporo, Japan, 26–29 May 2019; Volume 2019. [CrossRef]

87. Mai, R.; Yang, B.; Chen, Y.; Yang, N.; He, Z.; Gao, S. A Misalignment Tolerant IPT System with Intermediate Coils for Constant-Current Output. *IEEE Trans. Power Electron.* **2019**, *34*, 7151–7155. [CrossRef]

88. Wang, C.-S.; Stielau, O.H.; Covic, G.; Covic, G.A. Design considerations for a contactless electric vehicle battery charger. *IEEE Trans. Ind. Electron.* **2005**, *52*, 1308–1314. [CrossRef]

89. Elliott, G.A.J.; Covic, G.A.; Kacprzak, D.; Boys, J.T. A new concept: Asymmetrical pickups for inductively coupled power transfer monorail systems. *IEEE Trans. Magn.* **2006**, *42*, 3389–3391. [CrossRef]

90. Huh, J.; Lee, S.W.; Lee, W.Y.; Cho, G.H.; Rim, C.T. Narrow-width inductive power transfer system for online electrical vehicles. *IEEE Trans. Power Electron.* **2011**, *26*, 3666–3679. [CrossRef]

91. Shin, J.; Song, B.; Shin, S.; Chung, S.; Kim, Y.; Jung, G.; Jeon, S. Design of buried power line for roadway-powered electric vehicle system. In Proceedings of the 2013 IEEE Wireless Power Transfer, WPT 2013, Perugia, Italy, 15–16 May 2013; pp. 56–59. [CrossRef]

92. Huh, J.; Lee, W.; Choi, S.; Rim, C. A new cross-segmented power supply rail for roadway powered electric vehicles. In Proceedings of the Proceedings—2012 3rd IEEE International Symposium on Power Electronics for Distributed Generation Systems, PEDG 2012, Aalborg, Denmark, 25–28 June 2012; pp. 291–296. [CrossRef]

93. Nagendra, G.R.; Boys, J.T.; Covic, G.A.; Riar, B.S.; Sondhi, A. Design of a double coupled IPT EV highway. In Proceedings of the IECON Proceedings (Industrial Electronics Conference), Vienna, Austria, 10–13 November 2013; pp. 4606–4611. [CrossRef]

94. Xiang, L.; Sun, Y.; Tang, C.; Dai, X.; Jiang, C. Design of crossed DD coil for dynamic wireless charging of electric vehicles. In Proceedings of the 2017 IEEE PELS Workshop on Emerging Technologies: Wireless Power Transfer (WoW), Chongqing, China, 20–22 May 2017. [CrossRef]

95. Zhang, Z.; Pang, H.; Lee, C.H.T.; Xu, X.; Wei, X.; Wang, J. Comparative Analysis and Optimization of Dynamic Charging Coils for Roadway-Powered Electric Vehicles. *IEEE Trans. Magn.* **2017**, *53*, 9402106. [CrossRef]

96. Kutkut, N.H.; Klontz, K.W. Design considerations for power converters supplying the SAE J-1773 electric vehicle inductive coupler. In Proceedings of the Conference Proceedings—IEEE Applied Power Electronics Conference and Exposition—APEC, Atlanta, GA, USA, 27 February 1997; Volume 2, pp. 841–847. [CrossRef]

97. International Commission on Non-Ionizing Radiation Protection. Icnirp guidelines for limiting exposure to time-varying electric and magnetic fields (1 hz–100 khz). *Health Phys.* **2010**, *99*, 818–836. Available online: https://www.icnirp.org/cms/upload/publications/ICNIRPLFgdl.pdf (accessed on 12 May 2021). [CrossRef]

98. International Commission on Non-Ionizing Radiation Protection. Icnirp Guidelines on Limits of Exposure to Static Magnetic Fields. *Health Phys.* **2009**, *96*, 504–514. Available online: https://www.icnirp.org/cms/upload/publications/ICNIRPstatgdl.pdf (accessed on 12 May 2021). [CrossRef] [PubMed]

99. Leaf Car Configurator | Leaf Electric Cars | Nissan UK. Available online: https://www.nissan.co.uk/vehicles/new-vehicles/leaf/configurator.html#configure/BAVi/A/version (accessed on 13 May 2021).

100. Choi, S.Y.; Gu, B.W.; Jeong, S.Y.; Rim, C.T. Advances in wireless power transfer systems for roadway-powered electric vehicles. *IEEE J. Emerg. Sel. Top. Power Electron.* **2015**, *3*, 18–36. [CrossRef]

101. Quinn, J.C.; Limb, B.J.; Pantic, Z.; Barr, P.; Zane, R. Techno-economic feasibly and environmental impact of wireless power transfer roadway electrification. In Proceedings of the 2015 IEEE Wireless Power Transfer Conference (WPTC), Boulder, CO, USA, 13–15 May 2015. [CrossRef]

102. Lukic, S.; Pantic, Z. Cutting the Cord: Static and Dynamic Inductive Wireless Charging of Electric Vehicles. *IEEE Electrif. Mag.* **2013**, *1*, 57–64. [CrossRef]

103. Why Get Wireless EV Charging? | Plugless. Available online: https://www.pluglesspower.com/learn-about-plugless-2/ (accessed on 13 May 2021).

104. Xian, Z.; Wang, G. Optimal dispatch of electric vehicle batteries between battery swapping stations and charging stations. In Proceedings of the IEEE Power and Energy Society General Meeting, Boston, MA, USA, 17–21 July 2016; Volume 2016. [CrossRef]